

Article

Modulating the Framework Negative Charge Density in the System [BDT-TTP]/[ReSCI]/[Re(S/Se)Cl]/[ReSCI]: Templating by Isosteric Cluster Anions of Identical Symmetry and Shape, Variations of Incommensurate Band Filling, and Electronic Structure in 2D Metals

Sandrine Perruchas, Kamal Boubekeur, Enric Canadell, Yohji Misaki, Pascale Auban-Senzier, Claude Pasquier, and Patrick Batail

J. Am. Chem. Soc., **2008**, 130 (11), 3335-3348 • DOI: 10.1021/ja074774s

Downloaded from <http://pubs.acs.org> on February 8, 2009



More About This Article

Additional resources and features associated with this article are available within the HTML version:

- Supporting Information
- Links to the 2 articles that cite this article, as of the time of this article download
- Access to high resolution figures
- Links to articles and content related to this article
- Copyright permission to reproduce figures and/or text from this article

[View the Full Text HTML](#)



ACS Publications
 High quality. High impact.

Modulating the Framework Negative Charge Density in the System $[\text{BDT-TTP}^+]/[\text{Re}_6\text{S}_5\text{Cl}_9^{1-}]/[\text{Re}_6(\text{S}/\text{Se})_6\text{Cl}_8^{2-}]/[\text{Re}_6\text{S}_7\text{Cl}_7^{3-}]$: Templating by Isosteric Cluster Anions of Identical Symmetry and Shape, Variations of Incommensurate Band Filling, and Electronic Structure in 2D Metals

Sandrine Perruchas,[†] Kamal Boubekeur,[†] Enric Canadell,[‡] Yohji Misaki,[§]
Pascale Auban-Senzier,^{||} Claude Pasquier,^{||} and Patrick Batail^{*†}

Laboratoire de Chimie et Ingénierie Moléculaire, Université d'Angers, CNRS, 2 Boulevard Lavoisier, 49045 Angers, France, Institut de Ciència de Materials de Barcelona (CSIC), Campus de la UAB, 08193 Bellaterra, Spain, Department of Applied Chemistry, Faculty of Engineering, Ehime University, 3 Bunkyo-cho, Matsuyama 790-8577, Japan, and Laboratoire de Physique des Solides, Université de Paris-Sud, CNRS, Bâtiment 510, 91405 Orsay, France

Received June 29, 2007; E-mail: patrick.batail@univ-angers.fr

Abstract: A series of 2D metals, β -(BDT-TTP)₆[Re₆Se₆Cl₈](CHCl₂-CHCl₂)₂, **2**; β -(ST-TTP)₆[Re₆S₆Cl₈](CH₂Cl-CHCl₂)₂, **3**; β -(BDT-TTP)₇[Re₆S₆Cl₈]_{0.5}[Re₆S₇Cl₇]_{0.5}(CH₂Cl₂), **4**; β -(BDT-TTP)₇[Re₆Se₆Cl₈]_{0.5}[Re₆S₇Cl₇]_{0.5}(CH₂Cl₂), **5**; β -(BDT-TTP)₈[Re₆S₇Cl₇](CH₂Cl₂)₄, **6** (BDT-TTP and ST-TTP are 2,5-bis(1,3-dithiol-2-ylidene)-1,3,4,6-tetrathiapentalene and 2-(1,3-diselenol-2-ylidene)-5(1,3-dithiol-2-ylidene)-1,3,4,6-tetrathiapentalene, respectively) is reported to have one single β -slab layered topology despite successive increases of the cluster anion negative charge. The charge density within the templating composite inorganic-neutral molecule slab is shown to remain above a threshold of ca. one negative charge per square nanometer, that is, for cluster anions with two negative charges and higher. Conversely, discrete stacks are shown to be stabilized instead in the semiconducting salts (BDT-TTP)₂[Re₆S₅Cl₉], **1** where the cluster anion bears one negative charge only. The electronic structure of salts **2–6** is shown to be very stable and kept almost intact across the series. The templating strategy is shown to fulfill its anticipated potential for deliberate installment of incommensurate band fillings in molecular metals. The deliberate admixture of the 6:1 and 8:1 structures yields novel phases with a 7:1 stoichiometry with the anticipated crystal and electronic structures. The action at the organic-inorganic interface triggered by changing the anion charge yet keeping its shape and volume identical, which ultimately governs the shape of the unit cell, is of paramount importance in defining the Fermi surface of these metallic salts. The present BDT-TTP salts thus provide a series of materials with strongly related but subtly different Fermi surfaces worthy of many physical studies. Shubnikov-de Haas measurements are expected to be particularly interesting since they are especially sensitive to the details of the Fermi surface.

Introduction

In 2000, we reported our findings that the composite inorganic cluster anion-neutral molecule single slabs within the layered hybrid metals β -(BDT-TTP)₆²⁺[(Re₆S₆Cl₈)²⁻(CH₂Cl-CHCl₂)₂] and β -(BDT-TTP)₆²⁺[(Mo₆Cl₁₄)²⁻(CH₂Cl-CHCl₂)₂] (Chart 1)¹ exhibit enough conformational flexibility to sustain the BDT-TTP β -slab topology (Chart 1) observed in the 2:1 series (BDT-TTP)₂X, X = ClO₄⁻, BF₄⁻, ReO₄⁻, PF₆⁻, AsF₆⁻, SbF₆⁻,² regardless of the inorganic cluster anion larger size and charge, simply by adjusting the net stoichiometry up to 6:1 and

incorporating a third molecule (from the electrocrystallization solvent) in the interstices between the bulkier cluster anions, isosteric to C₆₀. This, and the earlier completion of the series of tetraalkylammonium salts of isosteric, isostructural, and isoelectronic cluster anions, [Re₆Q_{8-n}Cl_{6+n}]ⁿ⁻⁴ (Q = S, Se), whose net charge may be varied from -1 ($n = 3$) to -4 ($n = 0$),³ inspired us to explore this system further to try and produce the full set of two-dimensional molecular hybrid metals reported herein where only the charge of the anion is changed keeping its shape and volume identical. Here, we report that the single

[†] Université d'Angers, CNRS.

[‡] ICMAB-CSIC, Bellaterra.

[§] Ehime University, Matsuyama.

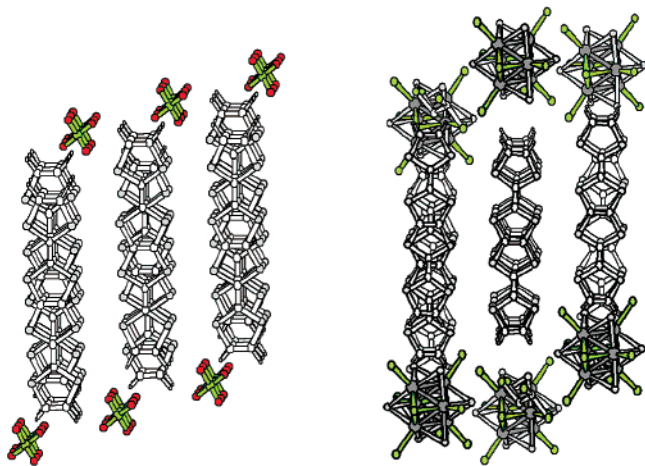
^{||} Université Paris-Sud, CNRS, Orsay.

(1) Deluzet, A.; Batail, P.; Misaki, Y.; Auban-Senzier, P.; Canadell, E. *Adv. Mater.* **2000**, *12*, 436.

(2) (a) Mori, T.; Misaki, Y.; Fujiwara, H.; Yamabe, T. *Bull. Chem. Soc. Jpn.* **1994**, *67*, 2685. (b) Kawamoto, Mori, T.; Yamaura, J.; Enoki, T.; Misaki, Y.; Yamabe, T.; Mori, H.; Tanaka, S. *Synth. Met.* **1997**, *1555*. (c) Misaki, Y.; Fujiwara, H.; Yamabe, T.; Mori, H.; Tanaka, S. *Chem. Lett.* **1994**, 1653.

(3) Gabriel, J.-C.; Boubekeur, K.; Uriel, S.; Batail, P. *Chem. Rev.* **2001**, *101*, 2037.

Chart 1. β -Type Organic Slab Topology of the 2:1 Salt (BDT-TTP)₂X, X = ClO₄⁻ (Left), Also Observed in the Hybrid Salt (BDT-TTP)₆²⁺·[(Re₆S₆Cl₈)²⁻·(CH₂Cl-CHCl₂)₂] (Right), Regardless of Its 6:1 Stoichiometry and the Larger Inorganic Cluster Anion Volume and Charge



β -slab layered topology distinctive of the rigid, fused-tetrathiafulvalene constituent is shown to be maintained⁴ throughout the series by adjusting the phase stoichiometries from 6 up to 7, then 8 radical cations per cluster anion upon successive increases of their negative charge, providing the charge density in the templating composite inorganic–neutral molecule slab remains above a threshold of ca. one negative charge per square nanometer. An in-depth analysis of the evolution of the electronic structure⁵ and transport properties is proposed with one dominant interrogation in mind: is the electronic structure kept intact across the series, and therefore, does the templating strategy fulfill its anticipated potential for deliberate installment of incommensurate band fillings in molecular metals?^{6–8} Strategies for the control of the electronic band structure and band filling by chemical means⁹ in molecular metals are much needed in order to meet expectations formulated in the context of remarkable recent progress in the physics of strongly correlated systems in low dimension.^{6–8}

Experimental Section

Electrocrystallization Experiments. Solvents used were freshly distilled. All compounds, whose formulation is summarized in Table 1, were obtained as high quality, dark brown plate-like single crystals. These crystals were grown at 30 °C in a two-compartment cell equipped with platinum electrodes ($l = 2$ cm, $\varnothing = 1$ mm), over a period of 12 days upon electrolysis¹⁰ at constant current ($0.4 \mu\text{A}\cdot\text{cm}^{-2}$). The cell was filled with solutions of (*n*-Bu₄N)[Re₆S₅Cl₉]¹¹ (25 mg) for **1**; of (*n*-Bu₄N)₃[Re₆S₇Cl₇]¹³ (20 mg) for **6** dissolved in dichloromethane (15 mL); of (*n*-Bu₄N)₂[Re₆S₆Cl₈] (25 mg) dissolved in 1,1,2-trichloroethane

(15 mL) for **3**; of (*n*-Bu₄N)₂[Re₆Se₆Cl₈]¹² (20 mg) for **2**; of equimolar amounts of (*n*-Bu₄N)₂[Re₆S₆Cl₈] (10 mg) and (*n*-Bu₄N)₃[Re₆S₇Cl₇] (11 mg) for **4**; and of (*n*-Bu₄N)₂[Re₆Se₆Cl₈] (10 mg) and (*n*-Bu₄N)₃[Re₆S₇Cl₇] (10 mg) for **5**, dissolved in a mixture of dichloromethane (7.5 mL) and 1,1,2-trichloroethane (7.5 mL). BDT-TTP¹⁴ (6 mg) and ST-TTP¹⁵ (7 mg) were introduced as solids in the anodic compartment. The π -donor molecules (drawn and formulated in Table 1) and the tetrabutylammonium salts of the rhenium chalcogenide cluster anions described in Chart 2 were prepared as described in the relevant references.

Single-Crystal X-ray Diffraction. X-ray data were collected at ambient temperature on a Stoe IPDS single ϕ axis diffractometer with a 2D area detector based on imaging plate technology with Mo K α radiation ($\lambda = 0.71073 \text{ \AA}$) (Stoe & Cie GmbH, *User's Manual V2.87*; Darmstadt, Germany, 1997). The structures were solved by direct methods (SHELXS-86) (G. M. Sheldrick, SHELXS-86, *Program for Crystal Structure Solution*; University of Göttingen: Germany, 1986) and refined by full-matrix least-squares based on F^2 (SHELXL-97) (G. M. Sheldrick, SHELXL-97, *Program for Crystal Structure Refinement*; University of Göttingen: Germany, 1997). The crystallographic data are summarized in Table 2, and additional details are provided below. In all structures, anisotropic thermal parameters were adopted for all non-hydrogen atoms, whereas the hydrogen atoms were simply introduced in structure factor calculations at idealized positions.

Refinement specifics for **1**: $\mu(\text{MoK}\alpha) = 16.916 \text{ mm}^{-1}$. A total of 11 962 reflections were collected up to $\theta = 24.93^\circ$ of which 4229 are independent and 3322 are observed ($F^2_o > 2\sigma(F^2_o)$). Gave $R(\text{obs}) = 0.0421$ [$R(\text{all}) = 0.0512$] and $R_w(\text{obs}) = 0.0983$ [$R_w(\text{all}) = 0.1007$] for 253 parameters.

Refinement specifics for **2**: $\mu(\text{MoK}\alpha) = 9.579 \text{ mm}^{-1}$. A total of 27 589 reflections were collected up to $\theta = 25.72^\circ$ of which 10 040 are independent and 5134 are observed ($F^2_o > 2\sigma(F^2_o)$). Gave $R(\text{obs}) = 0.0380$ [$R(\text{all}) = 0.0875$] and $R_w(\text{obs}) = 0.0729$ [$R_w(\text{all}) = 0.0804$] for 622 parameters.

Refinement specifics for **3**: $\mu(\text{MoK}\alpha) = 11.174 \text{ mm}^{-1}$. A total of 11 031 reflections were collected up to $\theta = 25.78^\circ$ of which 10 255 are independent and 5134 are observed ($F^2_o > 2\sigma(F^2_o)$). Gave $R(\text{obs}) = 0.0373$ [$R(\text{all}) = 0.0881$] and $R_w(\text{obs}) = 0.0785$ [$R_w(\text{all}) = 0.0875$] for 600 parameters.

Refinement specifics for **4**: $\mu(\text{MoK}\alpha) = 6.752 \text{ mm}^{-1}$. A total of 32 985 reflections were collected up to $\theta = 25.89^\circ$ of which 11 858 are independent and 7010 are observed ($F^2_o > 2\sigma(F^2_o)$). Gave $R(\text{obs}) = 0.0395$ [$R(\text{all}) = 0.0753$] and $R_w(\text{obs}) = 0.1004$ [$R_w(\text{all}) = 0.1063$] for 686 parameters.

Refinement specifics for **5**: $\mu(\text{MoK}\alpha) = 7.285 \text{ mm}^{-1}$. One CH₂-Cl₂ molecule was located and included in the refinements. The observed significant disorder precluded any further attempts at modeling the presence of eventually mixtures of dichloromethane and trichloroethane. A total of 33 066 reflections were collected up to $\theta = 25.88^\circ$ of which 11 870 are independent and 6417 are observed ($F^2_o > 2\sigma(F^2_o)$). Gave $R(\text{obs}) = 0.0445$ [$R(\text{all}) = 0.0890$] and $R_w(\text{obs}) = 0.1174$ [$R_w(\text{all}) = 0.1275$] for 690 parameters.

Refinement specifics for **6**: $\mu(\text{MoK}\alpha) = 6.481 \text{ mm}^{-1}$. One CH₂-Cl₂ molecule was located and included in the refinements. The observed significant disorder precluded any further attempts at modeling the presence of eventually mixtures of dichloromethane and trichloroethane. A total of 34 795 reflections were collected up to $\theta = 25.94^\circ$ of which 12 860 are independent and 9219 are observed ($F^2_o > 2\sigma(F^2_o)$). Gave $R(\text{obs}) = 0.0484$ [$R(\text{all}) = 0.0709$] and $R_w(\text{obs}) = 0.1451$ [$R_w(\text{all}) = 0.1522$] for 793 parameters.

(4) Conversely, note that diversity in dimensionality and topology is the rule when templating the flexible radical cation TTF-(CH₂OH)₄^{•+} by the same cluster series: Perruchas, S.; Boubekour, K.; Batail, P. *Cryst. Growth Des.* **2005**, *5*, 1585.

(5) Rousseau, R.; Gener, M.; Canadell, E. *Adv. Funct. Mater.* **2004**, *14*, 201.

(6) Giamarchi, T. *Chem. Rev.* **2004**, *104*, 5037.

(7) Giamarchi, T. *Quantum Physics in One Dimension*; Oxford University Press: Oxford, U.K., 2004.

(8) Seo, H.; Hotta, C.; Fukuyama, H. *Chem. Rev.* **2004**, *104*, 5005.

(9) (a) Mori, H.; Kamiya, M.; Haemori, M.; Suzuki, H.; Tanaka, S.; Nishio, Y.; Kajita, K.; Moriyama, H. *J. Am. Chem. Soc.* **2002**, *124*, 1251. (b) Mori, T. *Chem. Rev.* **2004**, *104*, 4947.

(10) Batail, P.; Boubekour, K.; Fourmigué, M.; Gabriel, J.-C. *Chem. Mater.* **1998**, *10*, 3005.

(11) Gabriel, J.-C.; Boubekour, K.; Batail, P. *Inorg. Chem.* **1993**, *32*, 2894.

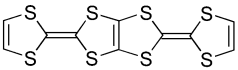
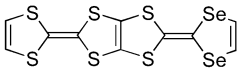
(12) Uriel, S.; Boubekour, K.; Gabriel, J.-C.; Batail, P.; Orduna, J. *Bull. Soc. Chim. Fr.* **1996**, *133*, 783.

(13) Guillaud, C.; Boubekour, K.; Gabriel, J.-C.; Batail, P. *C. R. Acad. Sci. Ser. IIc* **1998**, *1*, 765.

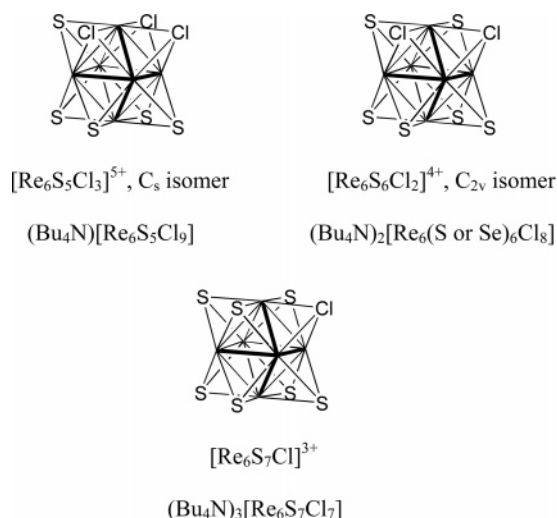
(14) Misaki, Y.; Matsui, T.; Kawakami, K.; Nishikawa, H.; Yamabe, T.; Shiro, M. *Chem. Lett.* **1993**, 1337–1340.

(15) Misaki, Y.; Kochi, T.; Yamabe, T.; Mori, T. *Adv. Mater.* **1998**, *10*, 588.

Table 1. Phase Summary and Single-Crystal Conductivity at Room Temperature

			$\sigma_{293\text{ K}}$ S cm ⁻¹
	BDT-TTP ^a	ST-TTP ^b	
(BDT-TTP) ₂ [Re ₆ S ₅ Cl ₉]	1		2
β -(BDT-TTP) ₆ [Re ₆ Se ₆ Cl ₈](CHCl ₂ -CHCl ₂) ₂	2		–
β -(BDT-TTP) ₆ [Re ₆ S ₆ Cl ₈](CH ₂ Cl-CHCl ₂) ₂	Ref 1		200
β -(BDT-TTP) ₆ [Mo ₆ Cl ₁₄](CH ₂ Cl-CHCl ₂) ₂	Ref 1		80
β -(ST-TTP) ₆ [Re ₆ S ₆ Cl ₈](CH ₂ Cl-CHCl ₂) ₂	3		600
β -(BDT-TTP) ₇ [Re ₆ S ₆ Cl ₈] _{0.5} [Re ₆ S ₇ Cl ₇] _{0.5} (CH ₂ Cl ₂)	4		80-800
β -(BDT-TTP) ₇ [Re ₆ Se ₆ Cl ₈] _{0.5} [Re ₆ S ₇ Cl ₇] _{0.5} (CH ₂ Cl ₂)	5		180
β -(BDT-TTP) ₈ [Re ₆ S ₇ Cl ₇](CH ₂ Cl ₂) ₄	6		200-1400

^a 2,5-Bis(1,3-dithiol-2-ylidene)-1,3,4,6-tetrathiapentalene. ^b 2-(1,3-Diselenol-2-ylidene)-5(1,3-dithiol-2-ylidene)-1,3,4,6-tetrathiapentalene.

Chart 2. Chalcogen/Halogen Proportion Distributed over the Eight μ_3 -Ligand Sites Capping the Faces of the Re₆ Octahedron Rules the Net Negative Charge of the Molecular Anion^a

^a Note that the six Re- μ -Cl have been omitted and that only one single isomer of the first two cores are represented. While the cluster cores are prepared as the Rb[Re₆S₅Cl₉],¹¹ Ca[Re₆S₆Cl₈],¹² Ca[Re₆Se₆Cl₈],¹² and Cs₃[Re₆S₇Cl₇]¹³ salts by high temperature solid-state reactions only, their alkylammonium salts provide access to their organic solution chemistry were hybrids may be assembled.

Determination of x by Microprobe Measurements, Occupancy Factors, Refinement Procedure, and Structure Analysis for (BDT-TTP)₇[Re₆S₆Cl₈] _{x} [Re₆S₇Cl₇]_{1- x} (CH₂Cl₂) **4, and (BDT-TTP)₇[Re₆Se₆Cl₈] _{x} [Re₆S₇Cl₇]_{1- x} (CH₂Cl₂) **5**.** In both structures, there is one-half independent cluster site occupied by both the [Re₆S₆Cl₈]²⁻ and [Re₆S₇Cl₇]³⁻ cluster anions in **4** and both the [Re₆Se₆Cl₈]²⁻ and [Re₆S₇Cl₇]³⁻ cluster anions in **5**.

For (BDT-TTP)₇[Re₆S₆Cl₈] _{x} [Re₆S₇Cl₇]_{1- x} (CH₂Cl₂) **4** the four independent, face-capping ligand sites where considered as sulfur atoms and refined accordingly; that is, the difference between sulfur and chlorine was considered to be negligible.

For (BDT-TTP)₇[Re₆Se₆Cl₈] _{x} [Re₆S₇Cl₇]_{1- x} (CH₂Cl₂) **5** the difference between sulfur and chlorine atoms has also been neglected

in the structure refinements. Only the occupancy factors of the selenium and chlorine atoms located on each of the four independent positions have been refined. The values obtained for selenium are 0.24, 0.34, 0.29, and 0.28. Averaging the former, independently refined occupancy factors over the four independent ligand sites, and taking into account the fact that all ligands are distributed over the eight face-capping ligand sites, the mixed selenium/cluster reads [Re₆Se_{2.3}Cl_{5.7}Cl₆] and the formulation for compound **5** reads (BDT-TTP)₇[Re₆Se₆Cl₈]_{0.38}[Re₆S₇Cl₇]_{0.62}(CH₂Cl₂) under the approximation conditions set in the refinement procedure. It is indeed important to note that all chlorine atoms have been refined throughout as sulfur atoms.

Microprobe experiments were carried out on single crystals of β -(BDT-TTP)₇[Re₆S₆Cl₈] _{x} [Re₆S₇Cl₇]_{1- x} (CH₂Cl₂) (Table S1) and β -(BDT-TTP)₇[Re₆Se₆Cl₈] _{x} [Re₆S₇Cl₇]_{1- x} (CH₂Cl₂) (Table S2) using a JEOL JSM-5800 LV to identify the presence of any amount of selenium atom and provide an independent, direct determination of the alloys formulation. No attempt was made at determining the actual chloride atom proportion on account of the uncertainty on the number of solvent molecules determined in the structure refinements. The analysis of the observed and calculated mass percentages collected in Table S2 are in agreement with $x = 0.5$, that is, with the presence of equimolar amounts of the two cluster anions in **5**. For **4**, only one single Re/S mass percentage is determined (Table S1), which in itself is not sufficient to determine by microprobe analysis a value for x for the [Re₆S₆Cl₈]²⁻-[Re₆S₇Cl₇]³⁻ alloy **4**.

Therefore, the microprobe analysis for **5** yields $x = 0.5$, to be compared to $x = 0.38$, estimated in the structure refinements. Note again that, for **4**, only the determination by microprobe analysis of the S/Re ratio is meaningful and that this does not allow for a characterization of the cluster anion proportion.

In addition, the analysis of the Re- μ -Cl bond lengths (the distances between the rhenium atoms and the outer, terminal halides has been proven to be sensitive to and to be a reliable probe of the cluster anion charge across many examples in these chalcohalide cluster series) also indicates that $x = 0.5$ for both **4** and **5**. Note also that, **4** and **5** being isostructural, the same x value is typically expected for both.

Note finally that the nominal proportion of [Re₆S₆Cl₈]²⁻ and [Re₆S₇Cl₇]³⁻ cluster anions and of [Re₆Se₆Cl₈]²⁻ and [Re₆S₇Cl₇]³⁻ cluster anions in the electrocrystallization cells for **4** and **5**, respectively,

Table 2. Summary of Crystallographic Data^a

	1	2	3	4	5	6
formula	C ₂₀ H ₈ Cl ₉ Re ₆ S ₂₁	C _{21.33} H ₁₀ Cl _{4.67} -Re ₂ S ₁₆ Se ₂	C ₆₄ H ₃₀ Cl ₁₄ Re ₆ S ₄₂ Se ₁₂	C ₇₁ H ₃₀ Cl ₈ Re ₆ S ₆₄	C ₇₁ H ₃₀ Cl ₁₄ Re ₆ S ₅₆ Se ₂	C ₈₄ H ₄₀ Cl ₁₅ Re ₆ S ₇₁
fw	2357.77	1475.01	4706.42	4335.59	4449.73	4974.37
T, K	293	293	293	293	293	293
space group	<i>P</i> $\bar{1}$	<i>P</i> $\bar{1}$	<i>P</i> $\bar{1}$	<i>P</i> $\bar{1}$	<i>P</i> $\bar{1}$	<i>P</i> $\bar{1}$
Z	1	1	1	1	1	1
a, Å	8.7677(12)	11.3494(9)	11,4947(11)	11.5401(12)	11.5650(12)	12.6588(11)
b, Å	11.3403(15)	12.6428(9)	12,7948(11)	13.4522(14)	13.4175(15)	13.9062(13)
c, Å	13.3801(19)	22.2207(18)	22,1584(18)	22.2800(20)	22.3340(20)	21.5140(20)
α , deg	65.288(15)	94.097(9)	94,162(10)	74.815(12)	74.967(12)	73.416(11)
β , deg	88.908(17)	100.051(10)	100,039(10)	80.498(12)	80.415(12)	81.642(11)
γ , deg	76.609(16)	114.099(8)	114,313(10)	81.427(13)	81.408(13)	78.573(10)
V, Å ³	1171.1(3)	2829.5(4)	2886,3(4)	3271.7(6)	3279.7(6)	3541.9(6)
d _{calc} , g/cm ³	3.343	2.597	2.708	2.200	2.253	2.332
R1 (wR2), %	4.21 (9.83)	3.80 (7.29)	3.73 (7.85)	3.95 (10.04)	4.45 (11.74)	4.84 (14.51)

^a Obtained with a graphite-monochromated Mo K α ($\lambda = 0.710\ 73\ \text{\AA}$) radiation.

was set to 1:1. Thus, these facts support the values of $x = 0.5$ for both **4** and **5** and the reported formulations.

Band Structure Calculations. The tight-binding calculations used an extended Hückel type Hamiltonian.¹⁶ The off-diagonal matrix elements of the Hamiltonian were calculated according to the modified Wolfsberg–Helmholz formula.¹⁷ A basis set composed of double- ζ Slater type orbitals for C, S, and Se and single- ζ Slater type orbitals for H was used. The exponents, contraction coefficients, and atomic parameters were taken from previous work.¹⁸

Conductivity Experiments. Single crystals used for conductivity measurements are black and shiny thin rectangular platelets with a typical length and width of 1.0 and 0.4 mm, respectively, and a thickness on the order of, or even smaller than, 25 μm . Four-probe low frequency (40–70 Hz) ac-conductivity measurements were performed on single crystals with gold contacts evaporated on both sides of the samples. The conductivity was measured along the most-conducting direction (the length of the crystals) with a lock-in amplifier. The applied current used is very small in order to remain in the linear regime: 10 μA for the metallic compounds and 0.1 μA for the semiconducting one. Measurements were performed at ambient pressure, which implies the occurrence, in the metallic regime, of numerous jumps of the resistance during cooling, as always observed in organic compounds. These jumps are due to microcracks of the samples because of large differential thermal contraction between the contacts made with silver paste and the samples. The room-temperature single-crystal conductivity values are collected in Table 1; the large apparent range of values reported for different crystals in the same batch for **4** and **6** is explained as follows. Considering the dimensions of the crystals, the geometrical factor relating the resistance to the conductivity is not precisely known: the thickness is difficult to estimate, and the distance between voltage contacts can be shorter than the width of the gold deposit and than the width of the sample. Moreover, this last point favors the presence of an unnested voltage, i.e., not well-defined current lines in the crystal. This effect is commonly observed in 2D phases of molecular metals like (BEDT-TTF)₂X salts. In samples measured here, it amounts to a maximum of 20% of the normal voltage (with a small increase when cooling down). Finally, microcracks can also appear during the drying of the silver paste leading to an increase of the measured resistance even at room temperature. All these problems prevent us from giving an absolute determination of the conductivity and could explain disparities from sample to sample as the geometrical factor is no longer pertinent. This is a typical illustration of the challenges faced when conducting transport experiments on fragile molecular crystals.

Results and Discussion

From [Re₆S₆Cl₈]²⁻ and [Re₆Se₆Cl₈]²⁻ to [Re₆S₇Cl₇]³⁻: One Single Organic Slab Topology Sustains Negative Template Charge Increments. As exemplified in Figures 1 and 2, radical cation and inorganic cluster anion single slabs alternate along c in the structures of β -(BDT-TTP)₈[Re₆S₇Cl₇] \cdot (CH₂Cl)₄, **6**, a bi-continuous hybrid layered architecture common to β -(BDT-TTP)₆[Re₆S₆Cl₈] \cdot (CH₂Cl–CHCl₂)₂,¹ β -(BDT-TTP)₆[Mo₆Cl₁₄] \cdot (CH₂Cl–CHCl₂)₂,¹ β -(BDT-TTP)₆[Re₆Se₆Cl₈] \cdot (CH₂Cl–CHCl₂)₂, **2**; and β -(ST-TTP)₆[Re₆S₆Cl₈] \cdot (CH₂Cl–CHCl₂)₂, **3**. Focusing on Figure 3, the organic slab topology in **6** resembles that in β -(BDT-TTP)₆[Re₆Se₆Cl₈] \cdot (CH₂Cl–CHCl₂)₂, **2**, itself identical to that¹ found in β -(BDT-TTP)₆[Re₆S₆Cl₈] \cdot (CH₂Cl–CHCl₂)₂, and also resembles that of β -(ST-TTP)₆[Re₆S₆Cl₈] \cdot (CH₂Cl–CHCl₂)₂, **3**. In fact, a global reading of the set of four topologies represented in Figure 3 discloses that one common slab is footprinted across the series by diverse unit cells whose dimension and shape change with the stoichiometry and cluster anion charge. Thus, the successful synthesis of **6** by engaging the cluster anion [Re₆S₇Cl₇]³⁻ reveals that one increment of the cluster template negative charge induces a reconstruction or evolution of the two-dimensional organic–inorganic interface to allow for the embrace of two additional radical cations, pushing the stoichiometry from 6:1 up to 8:1. Yet, it is important to note that this evolution of the two-dimensional organic–inorganic interface essentially keeps with the same underlying organic slab pattern.

At this point, given the common organic slab topology and the evolving, yet closely related, organic–inorganic interface topologies revealed throughout **2** or **3** to **6** (Figure 4), as discussed further in the next section, it occurred to us that this common organic slab topology might in fact be patterned or footprinted yet again differently by another unit cell of another phase resulting in the deliberate admixture of the structures of compounds **2** (or **3**) and **6** upon engaging equimolecular amounts of (Bu₄N)₂[Re₆S₆Cl₈] or (Bu₄N)₂[Re₆Se₆Cl₈] and (Bu₄N)₃[Re₆S₇Cl₇] in the electrocrystallization cells. Hence, the new phases (BDT-TTP)₆₊₈⁽²⁺³⁾⁺[Re₆(S or Se)₆Cl₈]²⁻ [Re₆S₇Cl₇]³⁻ would be expected to form where the typical common organic β -slab topology would be unchanged, yet now accounted for by a novel unit cell encompassing seven radical cation molecules balancing one cluster anion whose averaged negative charge in the solid state would amount to 2.5.

(16) Whangbo, M.-H.; Hoffmann, R. *J. Am. Chem. Soc.* **1978**, *100*, 6093.

(17) Ammeter, J.; Bürgi, H.-B.; Thibault, J.; Hoffmann, R. *J. Am. Chem. Soc.* **1978**, *100*, 3686.

(18) (a) Pénicaud, A.; Boubekeur, K.; Batail, P.; Canadell, E.; Auban-Senzier, P.; Jerome, D. *J. Am. Chem. Soc.* **1993**, *115*, 4101. (b) Pénicaud, A.; Batail, P.; Coulon, C.; Canadell, E.; Perrin, C. *Chem. Mater.* **1990**, *2*, 123.

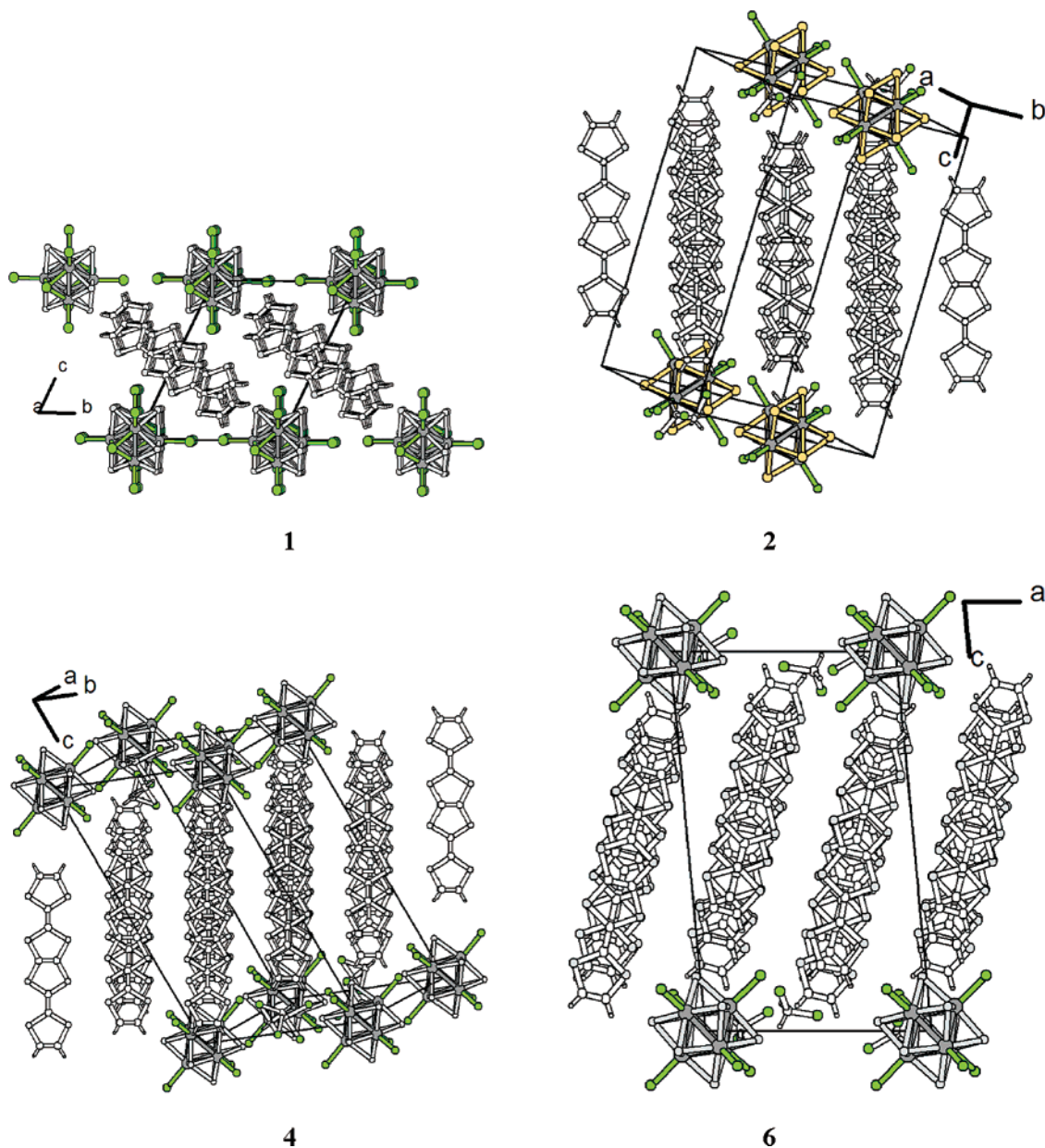


Figure 1. Discrete, essentially noninteracting radical cation single stacks are interspersed between piles of cluster monoanions in $(\text{BDT-TTP})_2[\text{Re}_6\text{S}_5\text{Cl}_9]$, **1**; Remarkably, when the negative charge of the cluster template increases as in $\beta\text{-(BDT-TTP)}_6[\text{Re}_6\text{Se}_6\text{Cl}_8]\cdot(\text{CH}_2\text{Cl}_2)_2$, **2**; $\beta\text{-(BDT-TTP)}_7[\text{Re}_6\text{S}_6\text{Cl}_8]_{0.5}[\text{Re}_6\text{S}_7\text{Cl}_7]_{0.5}\cdot(\text{CH}_2\text{Cl}_2)_4$, **4**; and $\beta\text{-(BDT-TTP)}_8[\text{Re}_6\text{S}_7\text{Cl}_7]\cdot(\text{CH}_2\text{Cl}_2)_4$, **6**, slabs of radical cations are stabilized. Then, two solvent molecules are anchored in a cavity in between four cluster anions.

This prediction proved to be fulfilled by the synthesis, phase formulation, and analysis of the crystal structures of $\beta\text{-(BDT-TTP)}_7[\text{Re}_6\text{S}_6\text{Cl}_8]_{0.5}[\text{Re}_6\text{S}_7\text{Cl}_7]_{0.5}\cdot(\text{CH}_2\text{Cl}_2)_4$, **4**, and $\beta\text{-(BDT-TTP)}_7[\text{Re}_6\text{S}_6\text{Cl}_8]_{0.5}[\text{Re}_6\text{S}_7\text{Cl}_7]_{0.5}\cdot(\text{CH}_2\text{Cl}_2)_4$, **5** (Figures 1, 3, and 4).

The analysis of the microprobe data (Tables S1 and S2) discussed in the Experimental Section provides evidence for the presence of equimolar proportions of $[\text{Re}_6\text{Se}_6\text{Cl}_8]^{2-}$ and $[\text{Re}_6\text{S}_7\text{Cl}_7]^{3-}$ in **5**. Obviously, the Re/S ratio itself is not sufficient to yield the same result for **4**. To that effect, another, complementary indication is proposed. It relies on an analysis of Re- μ -Cl bond lengths (Table 3). It is now well documented that the latter increases linearly with the net cluster charge in the series $[\text{Re}_6\text{S}_{8-n}\text{Cl}_{6+n}]^{n-4}$ ($n = 0-4$), as a result of a decreasing screening by less positively charged cluster cores.^{4,11}

Note that the Re- μ -Cl bond lengths are also sensitive to the cluster environment in the crystal (Figure 3).^{3,19} In the present series, however, the cluster environments are remarkably similar which makes the Re- μ -Cl bond length a reliable probe of the actual anion charge. The synthesis of **2** was carried out with precisely this in mind in order to provide for a reference for the Re- μ -Cl bond length in $[\text{Re}_6\text{Se}_6\text{Cl}_8]^{2-}$ in the very same environment in comparison to that in the adduct, $\beta\text{-(BDT-TTP)}_7[\text{Re}_6\text{S}_6\text{Cl}_8]_{0.5}[\text{Re}_6\text{S}_7\text{Cl}_7]_{0.5}\cdot(\text{CH}_2\text{Cl}_2)_2$, **5**. An analysis of the distances collected in Table 3 confirms the microprobe data analysis and cluster charge in all compounds, notably the formulations $\beta\text{-(BDT-TTP)}_7[\text{Re}_6\text{S}_6\text{Cl}_8]_{0.5}[\text{Re}_6\text{S}_7\text{Cl}_7]_{0.5}\cdot(\text{CH}_2\text{Cl}_2)_4$, **4**, and $\beta\text{-(BDT-TTP)}_8[\text{Re}_6\text{S}_7\text{Cl}_7]\cdot(\text{CH}_2\text{Cl}_2)_4$, **6**.

(19) Baudron, S. A.; Deluzet, A.; Boubekur, K.; Batail, P. *Chem. Commun.* **2002**, 2124.

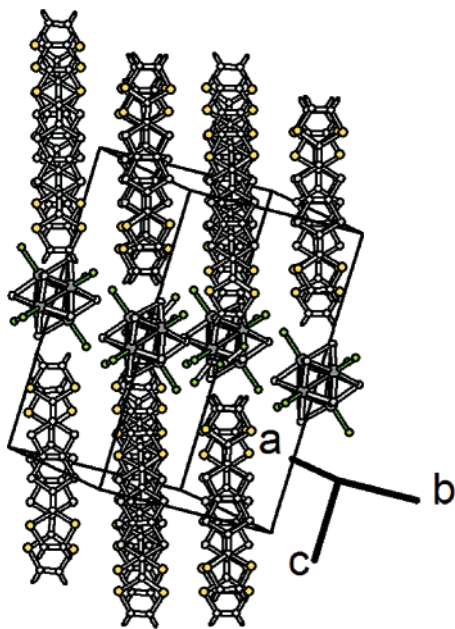


Figure 2. In β -(ST-TTP)₆[Re₆S₆Cl₈]·(CH₂Cl-CHCl₂)₂, **3**, the β -slab topology is maintained upon substitution of the outer sulfur for selenium (yellow) atoms in the donor molecule.

Cl₇)_{0.5}·(CH₂Cl)₂, **4**, and β -(BDT-TTP)₇[Re₆Se₆Cl₈]_{0.5}[Re₆S₇-Cl₇)_{0.5}·(CH₂Cl)₂, **5**.

Analysis of the Inorganic–Organic Interface: Negative Charge Density of the Inorganic Frame and π -Donor Footprints. A primary, local point of view is offered by inventorying all relevant intermolecular interactions defining the molecular embraces at the inorganic–organic interface. Regardless of the increase of both the cluster anion charge and number of radical cation molecules contributing to the interface, a consistent set of five C–H···Cl_{cluster} hydrogen bonds (Table S3), shown in Figure 4, is identified and qualifies the similarity in details noted earlier.

Another, complementary angle from which to analyze the inorganic–organic interface in the series is proposed in Table 4. It requires the comparison of two items. The first item is the negative charge density of the inorganic template unit frame. It is defined as the ratio of the net negative cluster anion charge over the inorganic template frame unit surface *absin* γ , expressed in nm². The second item is the π -donor footprints, expressed in nm² molecule⁻¹, defined as the ratio of the inorganic template frame unit surface to the number of π -donor molecules in the unit cell. Combining these two items allows for a perspective on the interface at a larger, nanometric scale, as exemplified in Table 4.

At the onset of this analysis it is of interest to consider the mixed valence salt (BDT-TTP)₂[Re₆S₅Cl₉], **1**. Crystals were successfully grown, in shear contrast with the failure to obtain a hybrid of this π -donor molecule with [Re₆S₈Cl₆]⁴⁻. As shown in Figures 1 and 5, dimerized, one-dimensional stacks of BDT-TTP are interspersed with cluster monoanions into a rather compact lattice, strikingly denser than any of the two-dimensional phases (Table 2). Thus, a structure dimensionality crossover has occurred in this hybrid composite for which the negative charge density within the most compact inorganic cluster frame unit amounts to one per square nanometer (Table 4). Of particular note in that respect is the observation in Table 4 that the two-dimensional β -slab topology achieved in all other

phases in the series is sustained by significantly higher negative charge densities, up to over 1.7 negative charge per square nanometer in **6**. The later, upper negative charge density value compares well with reference values determined for other prototypical systems like 1.7 and a footprint of 0.3 nm² molecule⁻¹ in β -(BEDT-TTF)₂I₃.²⁰ Note also that the higher negative charge density supported by the inorganic template frame is associated with the less compact lattice, as its density is the smallest (Table 2). This may be seen as a genuine manifestation of the hybrid character of these ionic–covalent molecular systems in which the dense mineral cluster cores are increasingly diluted in the solid by adding more π -conjugated molecules, in addition to solvent molecules in the interstices between the cluster anions.

For higher negative charge density of the inorganic cluster anion unit frames, here typically in the range 1.4–1.7 charges per square nanometer, more radical cation molecules reach out at the interface. As shown in Table 4, it is remarkable that one single π -donor footprint value, 0.2 nm² molecule⁻¹, is found for all two-dimensional systems in these series. Thus, upon increasing the negative charge density at the interface, the inorganic unit frame surface increases to allow for one, then two radical cations to reach out end-on at the interface. On the other hand, when the negative charge on the inorganic cluster anion unit frame is diluted down to one charge per square nanometer, fewer radical cations may be stabilized at the interface which they now approach side-on, imposing a larger footprint, here 0.5 nm² molecule⁻¹. Note that, the latter figures compare well with the negative charge density of 0.9 and footprint of 0.5 determined for κ -(BEDT-TTF)₂[Cu(N(CN)₂Br)].²¹ Hence, the observed dimensionality crossover which has occurred here may have been bypassed in the event of the stabilization of a two-dimensional slab of orthogonal dimers typical of the κ -phase topology, again underlining the complex balance of intermolecular interactions directing such molecular topologies.²²

Then, a question arises: is there an upper limit to the charge density that may be sustained at the interface of these two-dimensional hybrid systems? On the basis of these simple electrostatic considerations, engaging [Re₆S₈Cl₆]⁴⁻ is expected to yield a 10:1 formulation calling for an inorganic unit frame of 2.0 nm² supporting a charge density of 2.0 negative charges per square nanometer. These figures appear compatible with the stabilization of a hybrid formulated β -(BDT-TTP)₁₀[ReS₈-Cl₆], as they compare well with the negative charge density of the inorganic template unit frame and π -donor footprint for other two-dimensional systems such as β -(BDT-TTP)₂SbF₆,² 2.3 and 0.2; β'' -(BEDT-TTF)₄ dioxane [Re₆S₆Cl₈],²³ 1.9 and 0.3; α -(BEDT-TTF)₈[SiW₁₂O₄₀],²⁴ 2.1 and 0.2; or κ -(EDT-TTF)₈-[Ca₂(TeW₆O₂₄)]·15H₂O,²⁵ 2.2 and 0.3.

- (20) Yagubskii, E. B.; Schegolev, F.; Laukhin, V. N.; Kononovich, P. A.; Kartsovnik, M. V.; Zwarykina, A. V.; Buravov, L. I. *JETP Lett.* **1984**, *39*, 12.
- (21) Kini, A. M.; Geiser, U.; Wang, H. H.; Carlson, K. D.; Williams, J. M.; Kwok, W. K.; Vandervoort, K. G.; Thompson, J. E.; Stupka, D. L.; Jung, D.; Whangbo, M.-H. *Inorg. Chem.* **1990**, *29*, 2555.
- (22) Fourmigué, M.; Batail, P. *Chem. Rev.* **2004**, *104*, 5379.
- (23) Deluzet, A.; Rousseau, R.; Guilhaud, C.; Granger, I.; Boubekeur, K.; Batail, P.; Canadell, E.; Auban-Senzier, P.; Jérôme, D. *Chem.–Eur. J.* **2002**, *8*, 3884.
- (24) Davidson, A.; Boubekeur, K.; Pénicaut, A.; Auban, P.; Lenoir, C.; Batail, P.; Hervé, G. *J. Chem. Soc., Chem. Commun.* **1989**, 1373.
- (25) Boubekeur, K.; Riccardi, R.; Batail, P.; Canadell, E. *C. R. Acad. Sci. Paris, t. 1, Ser. IIc* **1998**, 627.

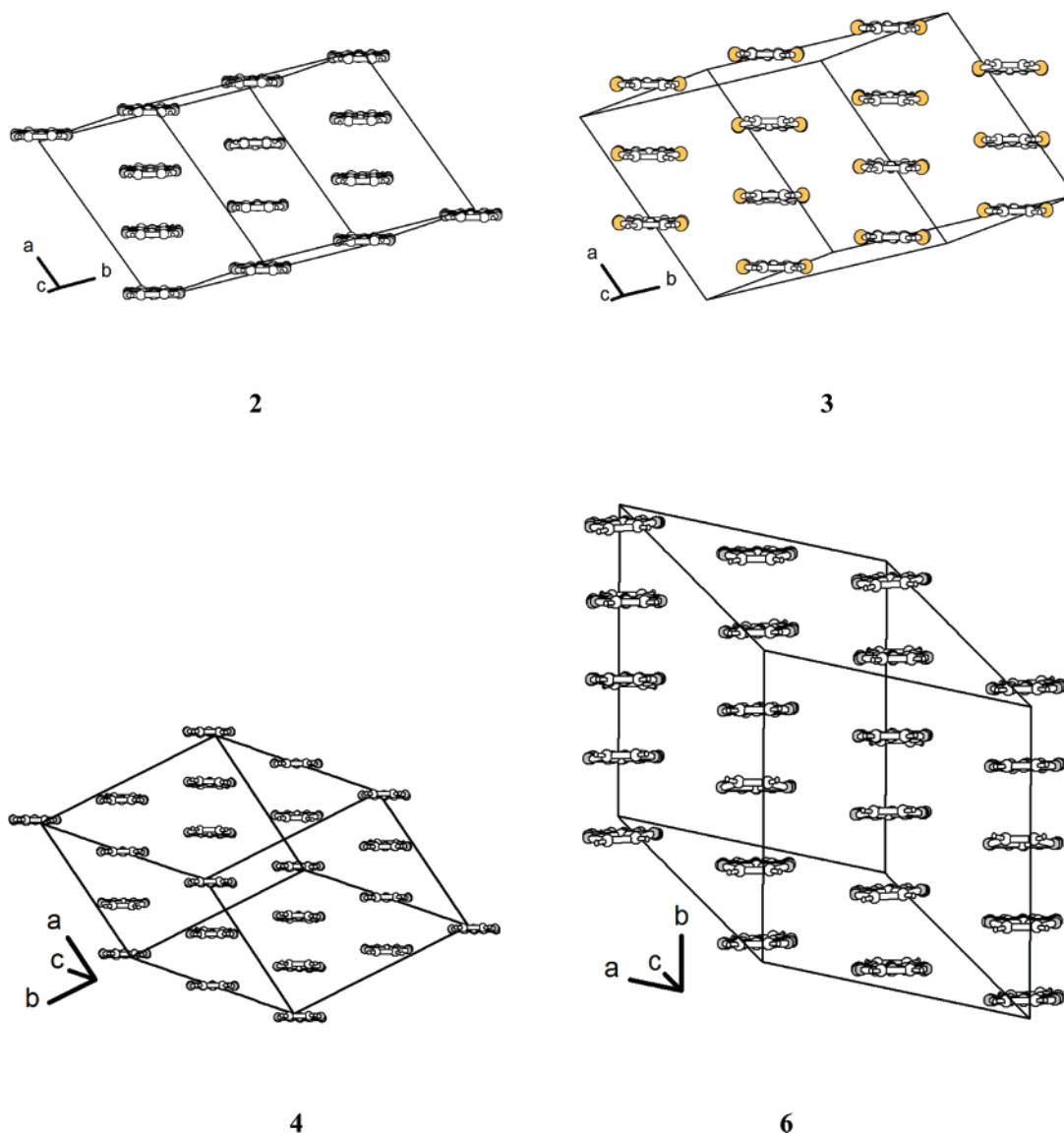


Figure 3. Compared projections down the long molecular axis of the single slabs in β -(BDT-TTP)₆[Re₆Se₆Cl₈](CHCl₂-CHCl₂)₂, **2**; β -(ST-TTP)₆[Re₆S₆-Cl₈](CH₂Cl-CHCl₂)₂, **3**; β -(BDT-TTP)₇[Re₆S₆Cl₈]_{0.5}[Re₆S₇Cl₇]_{0.5}(CH₂Cl)₂, **4**; and β -(BDT-TTP)₈[Re₆S₇Cl₇](CH₂Cl)₄, **6**. Note the singularity of the topography of the unit cell footprint onto the slab in **6** as it differs from the other three.

Finally, note that admixtures of mono- and dianionic clusters of these series have been identified earlier in Cs₅[Re₆S₅-Cl₉][Re₆S₆Cl₈]¹¹ and [bis(Me₂TTF)ethane]₅[Re₆Se₅Cl₉][Re₆Se₆-Cl₈].²⁶

One Common β -Type Topology and One Common Electronic Band Structure? Variations on a Theme. The structural analysis of the previous sections suggests that the β -type slabs of the new BDT-TTP salts reported here are very much alike. However, this observation does not necessarily mean that the details of the electronic structure, and hence the physical behavior, must also be very similar. Because of the intrinsic weakness of the intermolecular HOMO–HOMO interactions, the electronic structure of molecular conductors is susceptible to significant changes for apparently minor structural variations. This lies at the heart of the very rich variety of physical behavior for related families of salts or even for a given compound as a

function of pressure, temperature, band filling, etc. To carefully consider this point we have carried out a study of the band structure and Fermi surface of a broad series of BDT-TTP salts including all salts in Table 1 as well as (BDT-TTP)₂SbF₆^{2c} and (BDT-TTP)₂ClO₄.^{2a} Exactly the same computational details were used in the calculations so that all of these results are directly comparable.

Among all systems studied, salt **1** exhibits a distinct band structure in harmony with its different structural characteristics. There are two HOMO (highest occupied molecular orbital) bands clearly separated by a band gap somewhat larger than 0.5 eV. They show a relatively weak dispersion along the a^* -direction and a nil dispersion along the b^* -direction (the interactions are of course nil along the c -direction). The electron count is such that the lower band is full and the upper one must be only half-filled so that from a purely one-electron perspective the system should be metallic. However, Mott localization is well-known to strongly modify this picture in particular for half-

(26) Dolbecq, A.; Boubekeur, K.; Batail, P.; Canadell, E.; Auban-Senzier, P.; Coulon, C.; Lerstrup, K.; Bechgaard, K. *J. Mater. Chem.* **1995**, *5*, 1707.

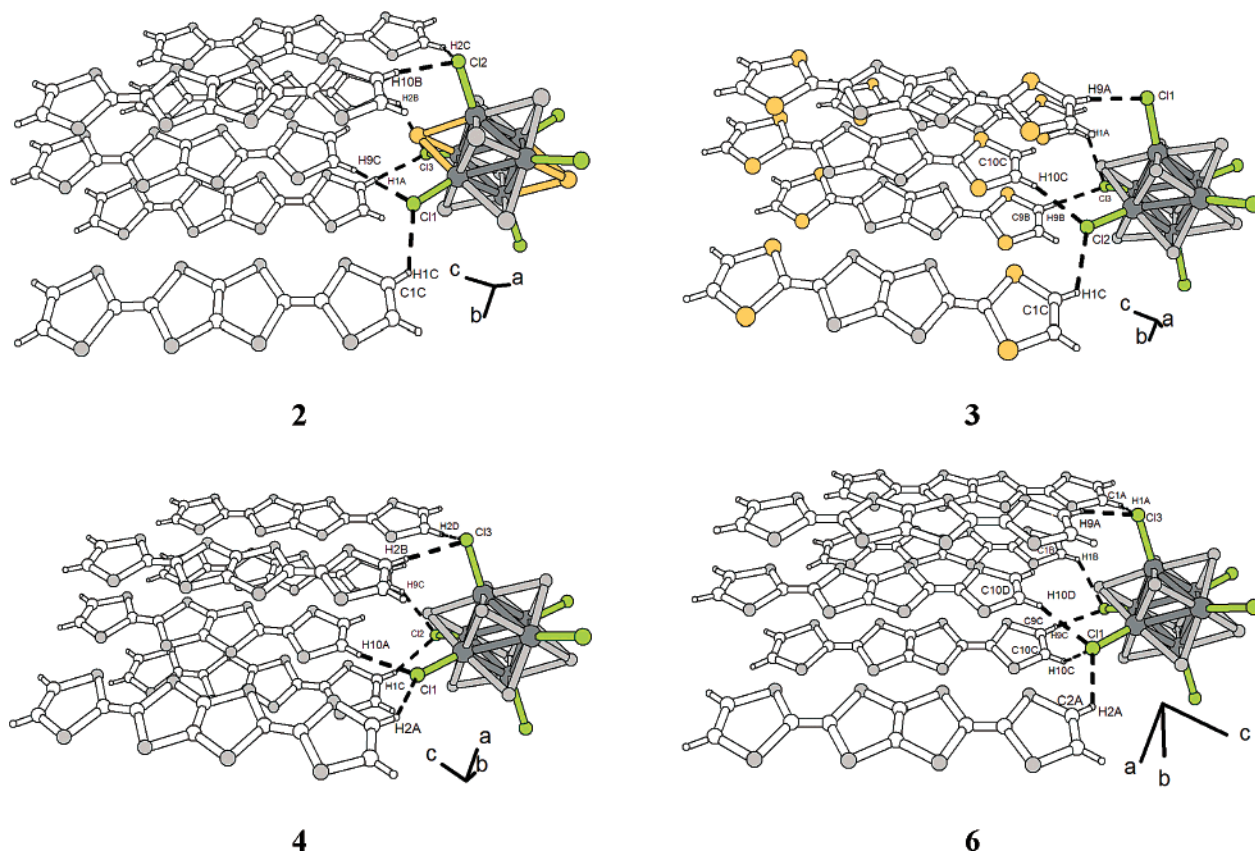


Figure 4. One single, consistent set of five C–H···Cl_{cluster} hydrogen bonds (Table S3) qualifies the molecular embraces at, and the similarity of, the inorganic–organic interface in β -(BDT-TTP)₆[Re₆Se₆Cl₈]·(CH₂Cl–CHCl₂)₂, **2**; β -(ST-TTP)₆[Re₆Se₆Cl₈]·(CH₂Cl–CHCl₂)₂, **3**; β -(BDT-TTP)₇[Re₆S₆Cl₈]_{0.5}[Re₆S₇Cl₇]_{0.5}·(CH₂Cl₂), **4**; and β -(BDT-TTP)₈[Re₆S₇Cl₇]·(CH₂Cl₂)₄, **6**.

Table 3. Evolution in the Series of the Re– μ -Cl Bond Lengths, Sensitive to the Cluster Anion Charge^a

	Re– μ -Cl (Å)			(Re– μ -Cl) (Å)
1	2.373(3)	2.367(2)	2.366(3)	2.369(3)
β -(BDT-TTP) ₆ [Re ₆ S ₆ Cl ₈] (CH ₂ Cl–CHCl ₂) ₂	2.372(2)	2.387(3)	2.382(2)	2.380(3)
2	2.378(2)	2.393(3)	2.389(3)	2.387(3)
4	2.402(3)	2.399(3)	2.388(3)	2.396(3)
5	2.402(4)	2.397(3)	2.394(4)	2.398(4)
6	2.401(3)	2.415(3)	2.413(3)	2.410(3)

^a Mean values are 2.344(45) Å for (Bu₄N)[Re₆S₅Cl₉][−]; 2.362(12) Å for (Bu₄N)₂[Re₆S₆Cl₈]^{2−}; 2.378(1) Å for (Bu₄N)₂[Re₆Se₆Cl₈]^{2−}; and 2.397(3) Å for (Bu₄N)₃[Re₆S₇Cl₇]^{3−}.^{3,11}

filled and relatively narrow band systems, and localization is therefore possible as observed (Figure 5b). The activation energy deduced from resistivity data amounts to $E_a = 670$ K at ambient pressure, a value comparable to the activation energy found in other strongly one-dimensional systems such as the well-known Fabre salt, (TMTTF)₂PF₆.²⁷ Here, however, the anion cluster volume is large and the system is barely compressible, as exemplified by the modest change of resistivity and activation energy observed (Figure 5b) between ambient pressure and 10 kbar. This clearly indicates that the electronic structure of this salt is essentially that of collections of radical cation dimers, (BDT-TTP₂)^{•+}, only slightly interacting along the chain direction *a*.

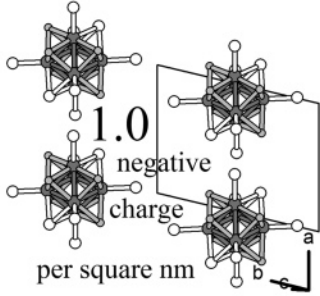
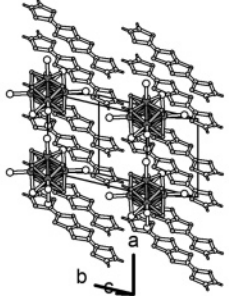
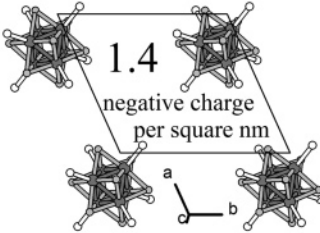
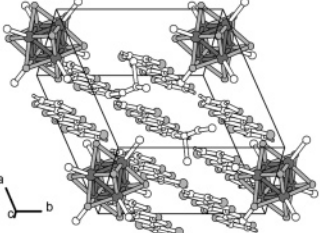
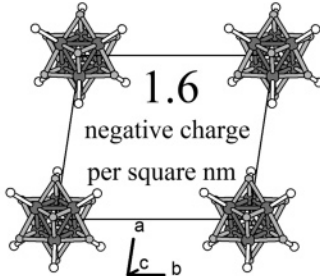
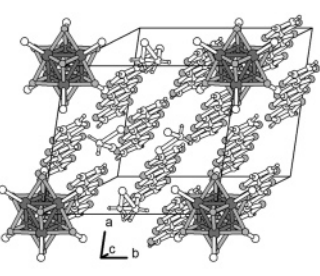
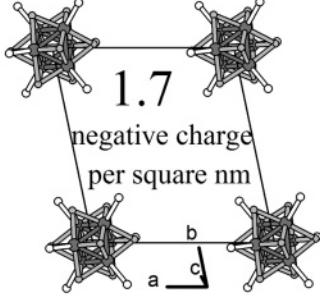
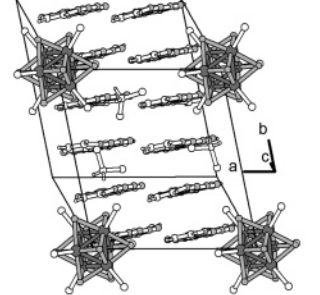
(27) Auban-Senzier, P.; Jérôme, D.; Carcel, C.; Fabre, J.-M. *J. Phys. IV (France)* **2004**, *114*, 4.

The calculated band structure near the Fermi level for a donor layer of salt **2** is shown in Figure 6a. There are six bands, mostly based on the HOMO of BDT-TTP, because there are six donor molecules per repeat unit of the slab. Because of the stoichiometry, 6:1, and the −2 charge of the anionic species, one of the six bands should be empty. However, the two upper bands overlap thus leading to two partially filled dispersive bands, and consequently, a metallic behavior is expected for this salt as observed¹ for β -(BDT-TTP)₆[Re₆S₆Cl₈]·(CH₂Cl–CHCl₂)₂. The calculated Fermi surface is reported in Figure 6b. Although this Fermi surface formally contains closed and open contributions, it is quite obvious that it results from the superposition and weak hybridization of a series of rounded rectangles. Thus, salt **2** is a typical two-dimensional metal with a Fermi surface strongly similar to the κ -(BEDT-TTF)₂X phases where large critical temperatures for superconductivity are observed. The calculated area of the closed orbit (α) of the Fermi surface is 18.1% of the cross section of the Brillouin zone in fair similarity with the area of the α -orbit of κ -(BEDT-TTF)₂Cu(NCS)₂ which covers 16% of the Brillouin zone.^{28,29} Such predictions might be verified through Shubnikov–de Haas measurements. Since the gaps between the closed and open portions are quite small it is likely that for relatively weak magnetic fields a magnetic breakdown phenomenon could be observed in these measurements. The associated Shubnikov–de Haas frequency would

(28) (a) Wosnitzer, J. *Fermi Surfaces of Low-Dimensional Metals and Superconductors*; Springer-Verlag: Berlin, Heidelberg, 1996. (b) Singleton, J. *Rep. Prog. Phys.* **2000**, *63*, 1111.

(29) Kartsovnik, M. V. *Chem. Rev.* **2004**, *104*, 5737.

Table 4. Elements for an Analysis of the Inorganic–Organic Interface (All Figures Are Projections onto the (a,b) Inorganic Cluster Anion Unit Frames)

	$(\text{BDT-TTP})_2$ $[\text{Re}_6\text{S}_5\text{Cl}_9], \mathbf{1}$	
inorganic template charge	1^-	
π -donor foot print ($\text{nm}^2 \text{mol}^{-1}$) ^a	0.5	
	$\beta(\text{BDT-TTP})_6$ $[\text{Re}_6\text{S}_6\text{Cl}_8]$ $(\text{CH}_2\text{Cl-CHCl}_2)_2, \mathbf{3}$	
inorganic template charge	2^-	
π -donor foot print ($\text{nm}^2 \text{mol}^{-1}$) ^a	0.2	
	$\beta(\text{BDT-TTP})_7$ $[\text{Re}_6\text{S}_6\text{Cl}_8]_{0.5}[\text{Re}_6\text{S}_7\text{Cl}_7]_{0.5}$ $(\text{CH}_2\text{Cl}_2)_4, \mathbf{4}$	
inorganic template charge	2.5^-	
π -donor foot print ($\text{nm}^2 \text{mol}^{-1}$) ^a	0.2	
	$\beta(\text{BDT-TTP})_8$ $[\text{Re}_6\text{S}_7\text{Cl}_7](\text{CH}_2\text{Cl}_2)_4, \mathbf{6}$	
inorganic template charge	3^-	
π -donor foot print ($\text{nm}^2 \text{mol}^{-1}$) ^a	0.2	

^a Defined as the ratio of the surface of the inorganic unit frame (that is, $ab \sin \gamma$), to the number of π -donor molecules in the unit cell.

correspond to the area of the parent rounded rectangle (β) which is exactly 100% of the cross section of the Brillouin zone. Quantum interference phenomena have also been observed in Fermi surfaces with this topology,³⁰ and thus, a low-temperature magnetoresistance study of this phase could be very interesting. For the other 6:1 salts studied, the calculated band structure and Fermi surfaces are extremely similar despite the substitution of two sulfur atoms by selenium atoms in the donor molecule in salt **3**. Likewise, the substitution of sulfurs for seleniums in the cluster anion does not affect the Fermi surface. The only appreciable difference is a slightly larger hybridization gap in

the Fermi surface of both **3** and $\beta(\text{BDT-TTP})_6[\text{Re}_6\text{Se}_6\text{Cl}_8](\text{CHCl}_2-\text{CHCl}_2)_2$, **2**, and, consequently, a slightly smaller area of the closed portion (α) of the Fermi surface in these salts, 14.8% and 16.4% of the cross section of the Brillouin zone, respectively.

The previous results suggest that for a given stoichiometry the electronic structure of these salts is very stable. Let us now consider a change in the stoichiometry. Shown in Figure 7 are the calculated Fermi surfaces for salts **4** (7:1 stoichiometry) and **6** (8:1 stoichiometry). The change in the stoichiometry can affect the Fermi surface in two different ways: (i) by changing the interactions at the interface and thus affecting the nature of the donor–donor interactions (i.e., the transfer integrals) and (ii) by changing the band filling. For instance, the average charge per donor is $+1/3$ for the 6:1 salts considered above but $+2.5/7$

(30) (a) Kartsovnik, M. V.; Logvenov, G. Yu.; Ishiguro, T.; Biberacher, W.; Anzai, H.; Kushch, N. D. *Phys. Rev. Lett.* **1996**, *77*, 2530. (b) Lyubovskii, R. B.; Pesotskii, S. I.; Gener, M.; Rousseau, R.; Canadell, E.; Perenboom, J. A. A. J.; Nizhankovskii, V. I.; Zhilyaeva, E. I.; Bogdanova, O. A.; Lyubovskaya, R. N. *J. Mater. Chem.* **2002**, *12*, 483.

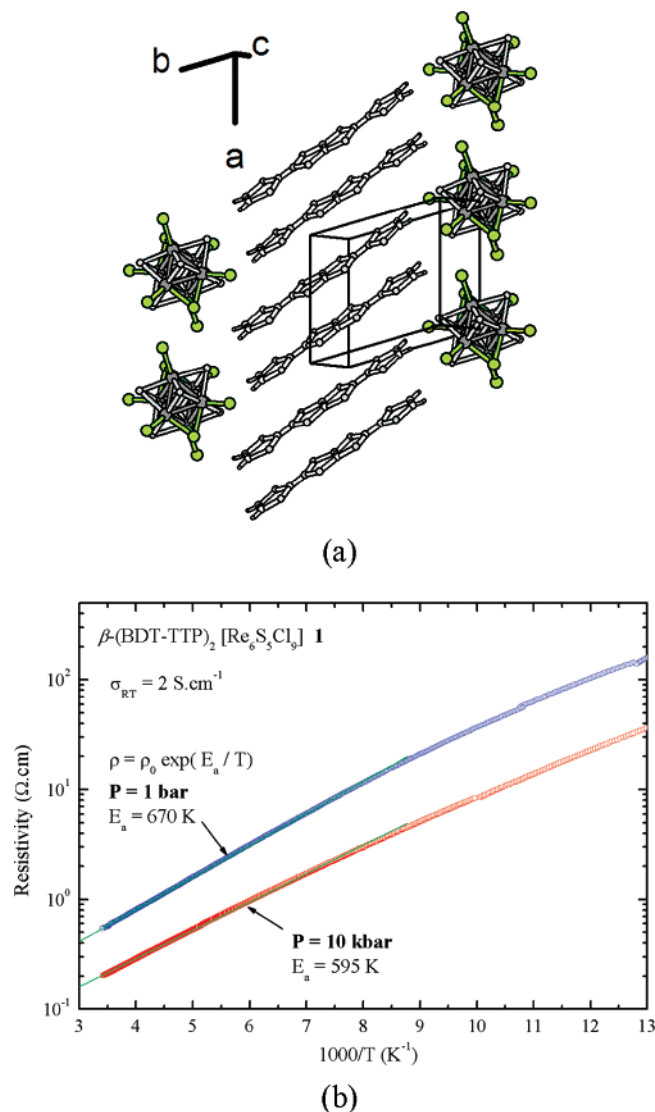


Figure 5. (a) One discrete stack in (BDT-TTP)₂[Re₆S₅Cl₉] **1**, where collections of dimers are only slightly interacting along *a*. (b) Temperature dependence of the resistivity for **1** at ambient pressure and 10 kbar, plotted as $\log(\rho)$ versus the inverse temperature, in order to get the activation energies. Note that only a modest decrease of the activation energy (fitted between 120 and 300 K, see the solid lines) occurs upon the application of 10 kbar of hydrostatic pressure, which demonstrates that the cluster anion framework is barely compressible.

$= +0.357$ for the 7:1 salts **4** and **5**, and $+3/8 = +0.375$ for the 8:1 salt **6**. The Fermi surface calculated for **4** (Figure 7a) is obviously very similar to those of the 6:1 salts. The only difference is the area of the rounded rectangle (β) which in this case corresponds to 125% of the cross section of the Brillouin zone (i.e., 2.5 holes here instead of 2 in the 6:1 salts) so that the overlap along the b^* -direction is larger than that in the 6:1 salts. Consequently, the area of the α orbit is also larger, now amounting to 36.8% of the cross-section of the Brillouin zone. Substitution of selenium for sulfur in the dianion does not change appreciably the Fermi surface; the only difference is a slightly larger gap between the closed and open portions. As noted above, salts with 7:1 stoichiometry have the interesting feature of having two anions with different charges but practically identical dimensions. This is an ideal situation for changing the band filling without altering the structure. Shown in Figure 8 are the calculated Fermi surfaces using a rigid band

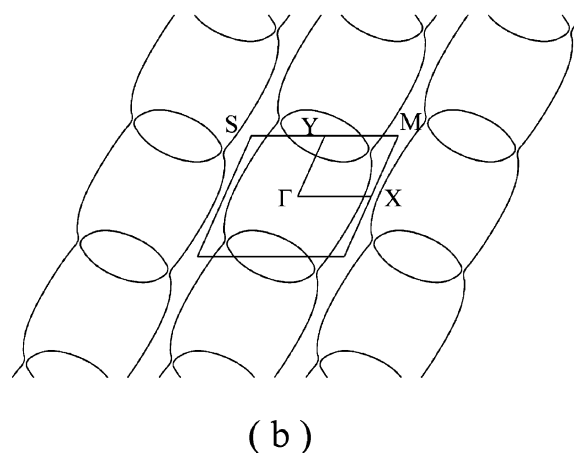
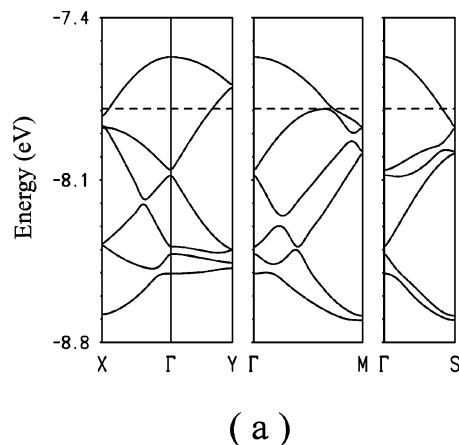


Figure 6. Band structure (a) and Fermi surface (b) for β -(BDT-TTP)₆[Re₆Se₆Cl₈] (CHCl₂-CHCl₂)₂ **2**, where $\Gamma = (0, 0)$, $X = (a^*/2, 0)$, $Y = (0, b^*/2)$, $M = (a^*/2, b^*/2)$, and $S = (-a^*/2, b^*/2)$. The dashed line in (a) refers to the Fermi level.

approach for the donor slabs of **4** corresponding to the hypothetical composition β -(BDT-TTP)₇[Re₆S₆Cl₈]_x[Re₆S₇-Cl₇]_{1-x}·(CH₂Cl₂). Changing the band filling from $x = 1$ (two holes in the HOMO bands) to $x = 0$ (three holes in the HOMO bands) does not change the shape of the Fermi surface except for the obvious increase of the area of the β orbit. Thus for any filling attainable through use of these octahedral rhenium clusters the shape of the Fermi surface does not qualitatively change. As shown in Figure 9, resistivity measurements confirm the metallic behavior down to the lowest temperature expected for **3**, **4**, and **5**. Indeed, Mott localization is much less pertinent as the band filling is no longer commensurate. Moreover, note the downward curvature of the resistivity observed below about 2 K for **4** (sample 2) (Figure 9b), a likely signature of superconducting fluctuations at low temperatures. This is not a true superconducting transition, as a weak magnetic field does not change the resistivity curve. The absence of a true superconducting transition may be related to the inherent disorder associated with the presence on the same site of two anions with different net negative charge densities as point disorder is known to reduce or even suppress the critical temperature for superconductivity.³¹

The Fermi surface for the 8:1 salt **6** is shown in Figure 7b. Surprisingly, the Fermi surface looks quite different, with two types of closed loops. Thus, it could be concluded that despite

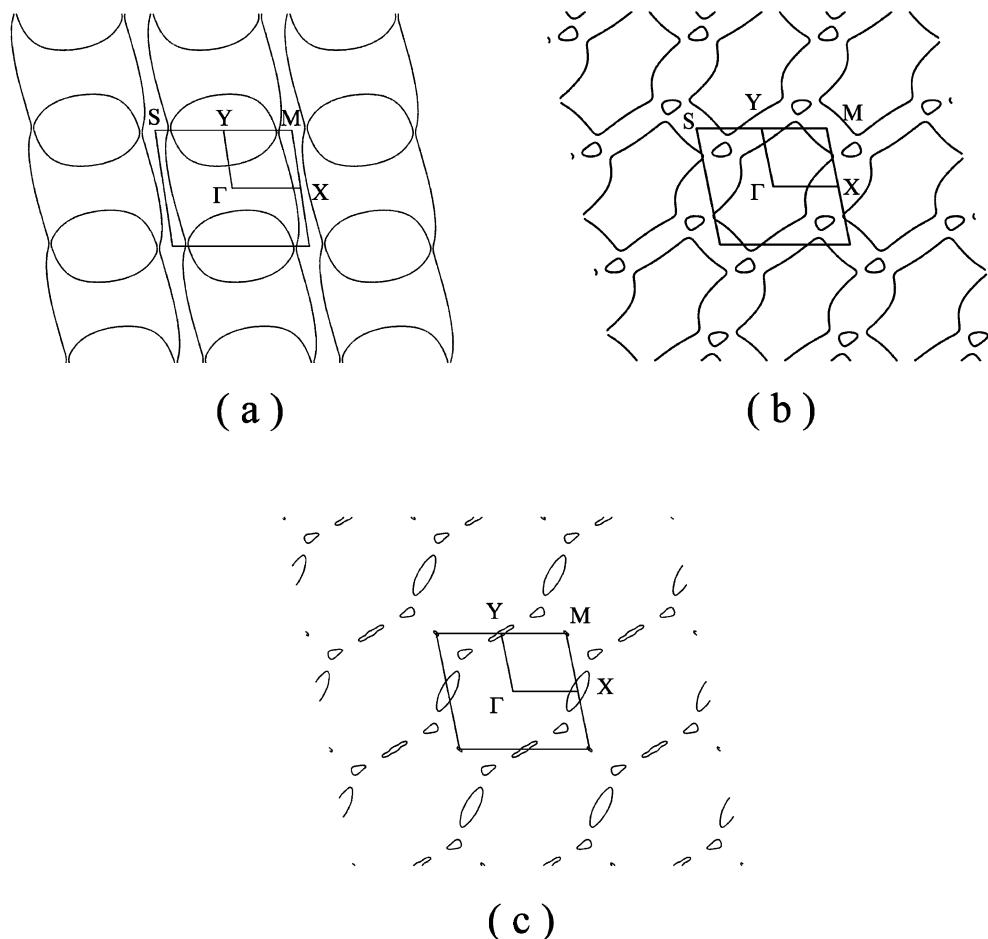


Figure 7. Calculated Fermi surface for β -(BDT-TTP)₇[Re₆S₆Cl₈]_{0.5}[Re₆S₇Cl₇]_{0.5}·(CH₂Cl₂)₄, **4**, (a) and β -(BDT-TTP)₈[Re₆S₇Cl₇]₁·(CH₂Cl₂)₄, **6**, (b), where $\Gamma = (0, 0)$, $X = (a^*/2, 0)$, $Y = (0, b^*/2)$, $M = (a^*/2, b^*/2)$, and $S = (-a^*/2, b^*/2)$. Shown in (c) is the Fermi surface for the donor layers of **6** assuming a rigid band scheme and two holes in the HOMO bands.

the structural similarity the electronic structure has been notably altered. This would not be quite correct. A careful look at this Fermi surface soon shows that, actually, it also results from a superposition of rounded rectangles which after hybridization lead to the Fermi surface of Figure 7b. There are two aspects to consider when comparing the changes between the Fermi surfaces of Figure 7a (or Figure 6b) and 7b. First, the pattern of superposition of the rounded rectangles has subtly changed, something which is related to the change in shape of the repeat unit of the layer. Second, the area of the rounded rectangle has increased when compared to the cross-sectional area of the Brillouin zone (i.e., there are three holes in the HOMO bands of **6** which is equivalent to 150% of this cross-sectional area vs 2.5 holes and 125% of the cross-sectional area in **4** and **5**). How do these two factors influence the shape of the Fermi surface of the 8:1 salt? To clarify this point we have carried out a computational experiment: using a rigid band approach we have calculated the Fermi surface assuming the existence of two holes in the HOMO bands. In that case the area of the rounded rectangle should be 100% of the cross section of the Brillouin zone. Let us recall that for the layers of the 7:1 compounds there is no qualitative variation when changing from three to two holes in the HOMO bands. In contrast, there is an important change for the 8:1 compound. Here, the Fermi surface (Figure

7c) is made up of a series of wavy lines of small closed pockets and minuscule pockets in between. The origin of this shape is not difficult to understand. The reduction of the number of holes and the concomitant decrease of the area of the rounded rectangle is such that, with the repetition pattern of salt **6**, the rounded rectangles overlap extensively (practically everywhere except at the rounded portions). As usually happens in this situation, the hybridization is strong and only small portions of the parent rounded rectangles survive as small closed pockets. This is not the case for the 7:1 (or 6:1) salts where the rounded rectangles overlap just around four points, and consequently they are easily recognizable even after the hybridization. Thus, in contrast with the case of the 7:1 and 6:1 salts, the Fermi surface of the 8:1 salt **6**, even if it also originates from the superposition of rounded rectangles, is (i) quite dependent on the electron filling and (ii) very different in shape than those of the 6:1 and 7:1 salts for comparable band fillings. The origin of these differences can be traced back to a subtle but purely structural aspect: the difference in shape of the repeat unit of the donor layer. As analyzed in detail elsewhere for the case of β'' -type donor layers,⁵ the Fermi surface of all these layers could be obtained from successive foldings of the Fermi surface of a parent layer with one donor per repeat unit and average transfer integrals (a rounded rectangle with a long axis slightly tilted along the direction of the step chains in these layers, i.e., for instance the *b*-direction in **3**; see Figure 3). The pattern of

(31) Joo, N.; Auban-Senzier, P.; Pasquier, C. R.; Jérôme, D.; Bechgaard, K. *Europhys. Lett.* **2005**, *72*, 645.

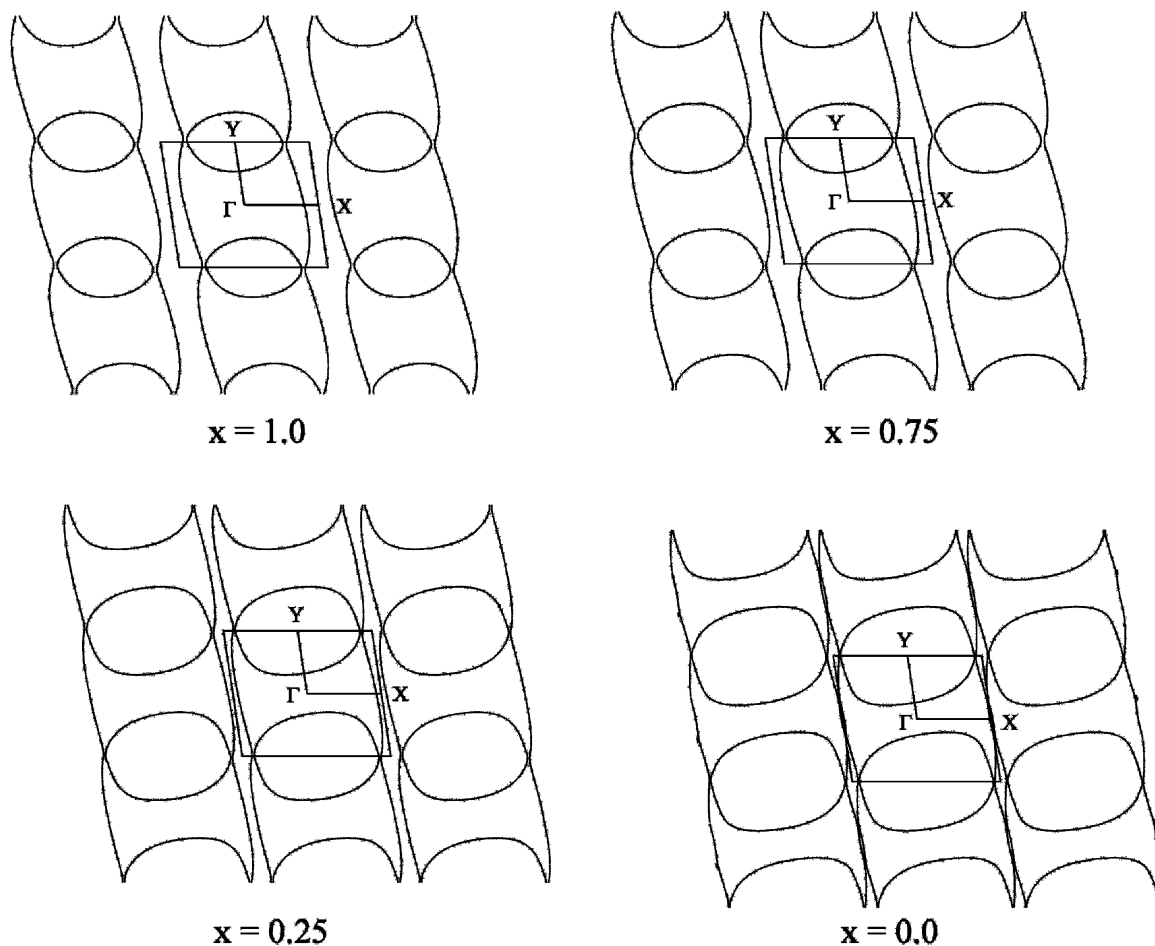


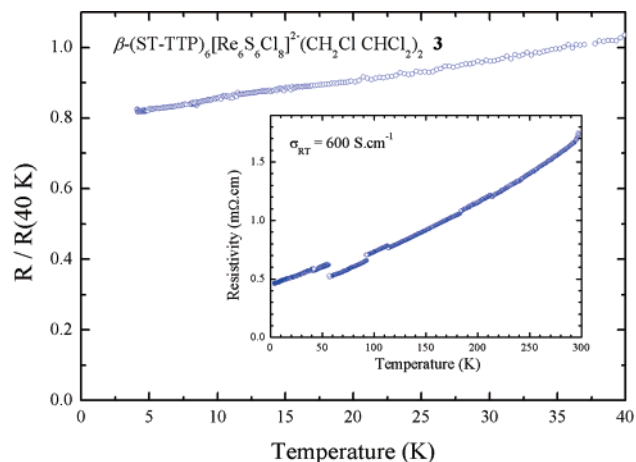
Figure 8. Calculated Fermi surface as a function of the band filling for β -(BDT-TTP)₇[Re₆S₆Cl₈]_x[Re₆S₇Cl₇]_{1-x}·(CH₂Cl₂)₄, **4**, assuming a rigid band approach. $\Gamma = (0, 0)$, $X = (a^*/2, 0)$, and $Y = (0, b^*/2)$.

superposition of this basic rounded rectangle is dictated by the repeat vectors of the Brillouin zone which themselves are imposed by the repeat vectors of the layer. Ultimately, it is the orientation of these vectors with respect to a fixed direction, say the long axis of the rounded rectangle, that determines the final shape of the Fermi surface for a given band filling.⁹ In the 6:1 and 7:1 salts, one of these vectors practically coincides with the long axis of the rounded rectangles leading to weak hybridization whatever the band filling; in the 8:1 salt **6** the overlap is different and may be considerably more extensive for some band fillings, leading to an instability of the shape of the Fermi surface. As shown by the resistivity measurements of Figure 10, a metallic behavior is observed for β -(BDT-TTP)₈·[Re₆S₇Cl₇]_{1-x}·(CH₂Cl₂)₄, **6**, in a wide range of temperature.

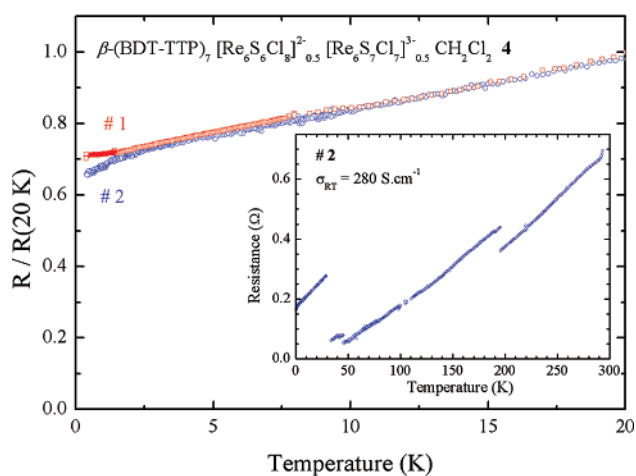
The action at the organic–inorganic interface triggered by changing the anion charge yet keeping its shape and volume identical, which ultimately governs the shape of the unit cell (Figure 3 and Table 4), and thus the repeat pattern of the basic motif, is of paramount importance in defining the Fermi surface of these metallic salts. It is worth mentioning, among the intriguing possibilities arising from this analysis, that changes in the shape of the “innocent”, space-filling partner, i.e., the solvent molecule, could change the shape of the repetition pattern and thus the Fermi surface;²³ it would also be interesting to see if, for a different space-filling neutral molecule, the shape

of the unit cell of salts **4** or **5** with a high content of the trianion would change to that in salt **6** or keep that of salts **4** and **5**.

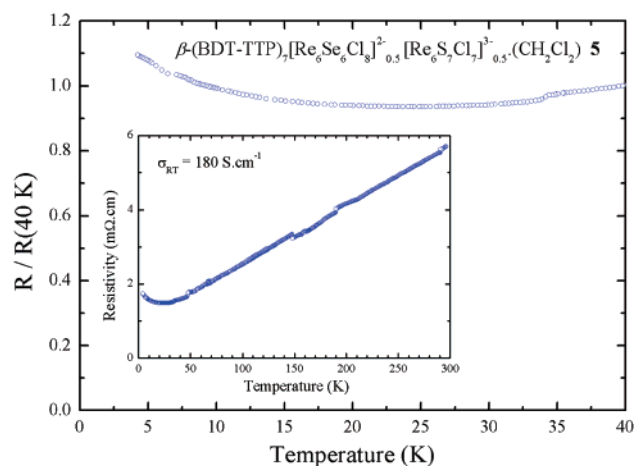
Before concluding this study let us briefly comment on the situation for salts in which the anion is smaller, such as (BDT-TTP)₂SbF₆ or (BDT-TTP)₂ClO₄.² These salts are also metallic down to very low temperatures. The donor layers of these two salts have the same topology as those discussed above. However, the repeat unit of the layers is different: that of the first salt is oblique and contains two donors, whereas that of the second is rectangular and contains four donors.^{2a,c} The calculated Fermi surface of the (BDT-TTP)₂SbF₆ salt is shown in Figure 11a. Although strictly speaking this Fermi surface is open, this is purely accidental. Since there are two donors with an average charge +1/2, there is one hole to be housed in the two HOMO bands. Consequently, if the Fermi surface is also built on the basis of a rounded rectangle, the associated area must be 50% of the cross section of the Brillouin zone. In fact, the Fermi surface of Figure 11a is exactly this. However, two of the vertices superpose practically at the border of the Brillouin zone, slightly hybridize, and create the small gaps. For slightly lower average charges, as for instance the hypothetical +3/8 charge characteristic of the previously discussed 8:1 salt, the number of holes is smaller leading to a rounded rectangle with a smaller area completely analogous to those discussed above (see Figure 11b). Note, however, that the repetition pattern of the rounded rectangles is different, a consequence of the different shape of



(a)



(b)



(c)

Figure 9. (a) Temperature dependence of the resistivity for **3**, normalized to 1 at 40 K. The insert shows the resistivity data up to room temperature; (b) Temperature dependence of the resistivity for two samples of **4**, normalized to 1 at 20 K. The insert shows the resistivity data for sample 2 up to room temperature; (c) Temperature dependence of the resistivity for **5**, normalized to 1 at 40 K. The insert shows the resistivity data up to room temperature.

the anion. The repeat unit of the donor layer in $(\text{BDT-TTP})_2\text{ClO}_4$ is twice as large, so that it is not surprising that the Fermi surface is essentially a folded version of the previous. The only variation

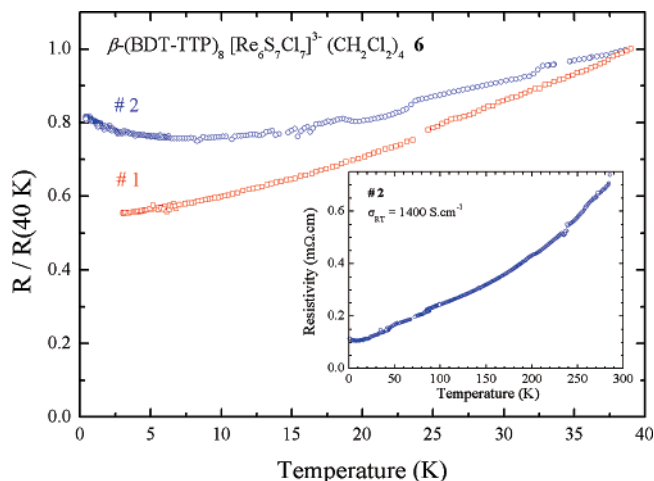
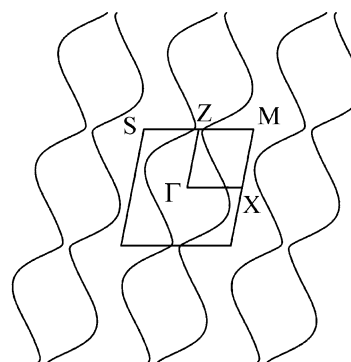
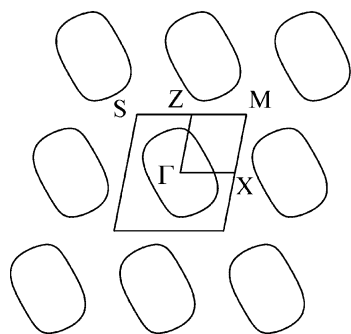


Figure 10. Temperature dependences of the resistivity for two samples of $\beta\text{-(BDT-TTP)}_8[\text{Re}_6\text{S}_7\text{Cl}_7](\text{CH}_2\text{Cl}_2)_4$, **6**. The insert shows the resistivity data for sample 2 up to room temperature.



(a)



(b)

Figure 11. (a) Calculated Fermi surface for $(\text{BDT-TTP})_2\text{SbF}_6$. (b) Fermi surface calculated assuming a rigid band scheme and an average $+3/8$ charge per donor. $\Gamma = (0, 0)$, $X = (a^*/2, 0)$, $Z = (0, c^*/2)$, $M = (a^*/2, c^*/2)$, and $S = (-a^*/2, c^*/2)$.

is that the rounded rectangle becomes almost a rounded square. Clearly, the electronic structure of these salts with smaller anions is completely analogous to those for the reported octahedral clusters anions.

Consequently, the answer to the question at the beginning of this section is affirmative: there is indeed one common β -type topology and one common electronic band structure. There are however many subtle variations on this common electronic

structure which are essentially driven by the apparently inert component of these conducting salts, i.e., the anion (and probably the solvent). Through its charge and shape, the anion imposes a definite type of organic–inorganic interface which enforces the shape of the unit cell of the salt and, thus, of the repeat unit of the donor layers. The repeat unit governs the repetition pattern of the rounded rectangular Fermi surface (with area imposed by the anion charge) which, after hybridization, leads to the real Fermi surface. The present BDT-TTP salts thus provide a series of materials with strongly related but subtly different Fermi surfaces worthy of many physical studies among which Shubnikov–de Haas measurements are expected to be particularly interesting since they are especially sensitive to the details of the Fermi surface.

Conclusion

The single β -slab layered topology distinctive of the rigid, fused-tetrathiafulvalene constituent has been shown to be maintained throughout the series by adjusting the phase stoichiometries from 6 up to 7, then 8 radical cations per cluster anion upon successive increases of their negative charge, providing the charge density in the templating composite inorganic–neutral molecule slab remains above a threshold of ca. one negative charge per square nanometer, that is, for cluster anions with two negative charges and higher. The foregoing in-depth analysis of the evolution of the electronic structure and transport properties demonstrates that for a given stoichiometry the electronic structure of these salts is very stable and kept intact across the series and, therefore, the templating strategy addressed at the onset of this study fulfills its anticipated potential for deliberate installment of incommensurate band fillings in molecular metals.

Two items have been proposed to analyze the inorganic–organic interface in the series: one is the negative charge density of the inorganic template unit frame, defined as the ratio of the net negative cluster anion charge over the inorganic template frame unit surface, expressed in square nanometers; the second item is the π -donor footprints, expressed in $\text{nm}^2 \text{molecule}^{-1}$, and defined as the ratio of the inorganic template frame unit surface to the number of π -donor molecules in the unit cell. It is further shown how this analysis sustained the successful prediction that the deliberate addition of the 6:1 and 8:1 structures would yield novel phases with a 7:1 stoichiometry and the anticipated crystal and electronic structures.

From the viewpoint of materials design and crystal engineering, it is exemplified herein that the action at the organic–inorganic interface triggered by changing the anion charge yet keeping its shape, symmetry, and volume identical, which ultimately governs the shape of the unit cell, and thus the repeat

pattern of the basic motif, is of paramount importance in defining the Fermi surface of these metallic salts. Of particular note is the intriguing possibilities arising from this analysis, that changes in the shape of the “innocent”, neutral space-filling partner, i.e., the solvent molecule, could change the shape of the repetition pattern and thus the Fermi surface. Future developments are anticipated in exploring the many subtle variations on this common electronic structure as being essentially driven by the apparently inert component of these conducting salts, i.e., the anion (and probably the solvent).

The present BDT-TTP salts thus provide a series of materials with strongly related but subtly different Fermi surfaces worthy of many physical studies among which Shubnikov–de Haas measurements are expected to be particularly interesting since they are especially sensitive to the details of the Fermi surface.

Finally, we note that the combined isostructural and isosteric, charge variable anion templating and phase summation approach described herein offers unique opportunities for the construction of many novel phases within the same prototypical incremental architecture by engaging numerous additional combinations of either one of the following molecular chalcogenide or chalcogenide cluster anions, $\text{Re}_6\text{Q}_5\text{X}_9^-$, $[\text{Re}_6\text{Q}_5\text{EX}_8]^{2-}$, $\text{Re}_6\text{Q}_7\text{X}_7^{3-}$, $\text{Re}_6\text{Q}_8\text{X}_6^{3-*}$, $\text{Re}_5\text{OsSe}_8\text{Cl}_6^{3-}$, ... or $\text{Re}_6\text{Q}_8\text{X}_6^{4-}$, (Q = S, E = O, S, Se; Q = Se, E = S, Se, Te; X = Cl, Br), or any of their binary, ternary, ... mixtures in diverse proportions. This is seen as an important step toward a novel approach to the materials chemistry and physics of designed metallic molecular compounds with tunable noncommensurate band fillings.

Acknowledgment. We thank the CNRS for support. Valuable insight from the late André Deluzet at the onset of this work is gratefully acknowledged as is the expert assistance from Jean-Charles Ricquier in preparing the TOC illustration. Work at Bellaterra was supported by MEC-Spain (Project FIS2006-12117-C04-01) and Generalitat de Catalunya (Project 2005 SGR 683). This work was partially supported by the 2002 A. de Betancourt - J. R. Perronet Prize of the Spanish Minister of Education (P.B.).

Supporting Information Available: Analysis of microprobe data for β -(BDT-TTP) $_7$ [$\text{Re}_6\text{S}_6\text{Cl}_8$] $_x$ [$\text{Re}_6\text{S}_7\text{Cl}_7$] $_{1-x}$ (CH_2Cl_2), **4** (Table S1); the analysis of microprobe data for β -(BDT-TTP) $_7$ -[$\text{Re}_6\text{Se}_6\text{Cl}_8$] $_x$ [$\text{Re}_6\text{S}_7\text{Cl}_7$] $_{1-x}$ (CH_2Cl_2), **5** (Table S2); the set of interfacial C–H \cdots Cl $_{\text{cluster}}$ hydrogen bonds in the series (Table S3); and the crystallographic information files (CIF). This material is available free of charge via the Internet at <http://pubs.acs.org>.

JA074774S